Dynamic Harmonic Analysis With FIR Filters Designed With O-Splines

José Antonio de la O Serna, *Senior Member, IEEE*

***Abstract*— Splines are at the essence of signal processing. Not only in sampling and interpolation, but also in filter design, image processing, and multi-resolution analysis. A new class of splines is presented here. They are referred to as O-splines since their knots are separated by one fundamental cycle. They are used as optimal state samplers, in the sense that their coefficients provide the derivatives for the best Taylor approximation to a given signal about a time instance or the best Hermite interpolation between two of them. They are the impulse response of the filters of the Discrete-Time Taylor-Fourier Transform (DTTFT) filter bank. Lowpass O-spline coincides with the Lagrange central interpolation kernel, which converges towards the ideal *Sinc* function. It comes with its derivatives which in turn converge to the ideal lowpass differentiator. The bandpass O-splines are harmonic splines since they are modulations of the former kernel at harmonic frequencies. In closed-form, they reduce the computational complexity of the DTTFT and can be used to design ideal bandpass filters at a particular frequency. By increasing the order they define a ladder of spaces very useful for multi-resolution and time-frequency analysis. Examples are provided at the end of the paper. Naturally, a new family of wavelets is coming soon from these splines.**

***Index Terms*— Splines, windows, interpolator-cardinal splines, Lagrange central interpolation kernel, Discrete Time Taylor-Fourier transform, oscillating signals, power oscillations, filter banks, blood pressure oscillometric waveforms, time-frequency analysis, multiresolution analysis, data compression.**

I. Introduction

SPLINES [1], [2] are not only at the basis of the essential digital signal processing operations such as sampling and interpolation, but also at filtering design [3], image processing [4], and multi-resolution analysis [5]. They have also been applied in computer-aided design and computer graphics to draw smooth curves with minimum curvature, and to reproduce graphical models and surface representation.

The best known splines in signal processing are the B-splines [6], [7]. B-splines of order m are continuous up to the $m-1$ derivative. This property guarantees interpolated curves with seamless junctions. They have compact support, but they are not themselves cardinal splines. However, they lay the foundation of the mathematical framework to design most of the modern interpolant cardinal splines, such as the so-called exponential B-splines or E-splines [8], [9], or linear combinations of them.

In this paper, a new class of splines is presented. O-splines were first obtained numerically in [10] to analyze power system oscillatory signals. They were also used to analyze electroencephalograms in [11]. Here they are given in closed-form to reduce the computational complexity in the analysis of band-limited signals.

O-splines are the impulse responses of the Discrete-Time Taylor-Fourier Transform (DTTFT) filter bank [10]. They are the dual functions of its signal model, which is a Taylor extension of the Discrete Fourier Transform (DFT), in which the Fourier coefficients are extended to Taylor polynomials. They are referred to as O-splines because they are cyclic, i.e. their knots are separated by intervals of one fundamental cycle, and because they provide optimal coefficients for the representation of functions in the DTTFT subspace.

O-splines in closed-form are obtained through the factorization of the DTTFT signal model into two operators: one with the Taylor terms, and the other with the Fourier complex exponentials. In this decomposition, lowpass O-splines and its derivatives are found in the dual matrix of the Taylor operator, and band-pass O-splines are simple harmonic modulations at the harmonic frequencies of the former ones.

The lowpass O-splines turn out to be given by the Lagrange central interpolation kernels, which have finite support and converge to the *Sinc* function as the order goes to infinity [12]. In consequence, their frequency responses converge to that of the ideal lowpass filter, and those of their derivatives to those of ideal lowpass differentiators.

Since O-splines operate in the analysis stage (dual matrix) [13], they perform together with their derivatives as optimal signal state samplers, in the sense that their coefficients at each time instance provide the signal derivatives for its best Taylor approximation given by the synthesis equation. This is an important difference with respect to most of the splines, whose literature is consecrated to their performance as interpolators [14].

The most recent example of cardinal interpolation splines are the many-knots (MK) splines [15]. They are symmetric FIR filters with samples at half-integers and obtained by a linear combination of the B-spline of the same order. They have two polynomial pieces per unit interval, with twice

Manuscript received March 3, 2020; revised April 11, 2020 and May 4, 2020; accepted May 19, 2020. Date of publication June 4, 2020; date of current version December 1, 2020. This work was supported by UANL under Paicyt project IT1051-19: "Comparative study of the spectral and interpolation properties of the O-splines and their derivatives." This article was recommended by Associate Editor M. Martina.

The author is with the Department of Electrical Engineering, UANL, San Nicolás de los Garza CP 66455, Mexico (e-mail: jdelao@ieee.org).

Color versions of one or more of the figures in this article are available online at https://ieeexplore.ieee.org.

Digital Object Identifier 10.1109/TCSI.2020.2996976

as many knots (hence its name) per unit interval. Even if MK- and O-splines share integer finite support, O-splines have nothing to do with B-splines. Their cardinality results directly from the adjoint operator of the Taylor-Fourier expansion. In consequence, O-splines are applied as sampling operators, the inverse of the interpolating ones. They obtain the best Taylor-Fourier coefficients, with physical meaning of position, speed, acceleration, etc. By being in the dual biorthogonal basis, they establish an hybrid analysis-synthesis process. These are the main distinctions that make O-splines unique, optimal, useful, and effective.

More recently, MK-splines were generalized into GMK-splines [16], an extensive family of splines, by relaxing the half-integers of the samples to rational numbers. Even if this relaxation produces some filters with non-flat passband gain and some with fractional (noninteger) support, the n-th order GMK splines have the continuity of order $n-1$.

DTTFT signal model was conceived as an extension from the traditional concept of phasor (Fourier coefficient) to the one of *dynamic phasor* for capturing oscillations with better accuracy. Its extended model corresponds to signals in the span$\{t^n e^{j2\pi h F_1 t}\}_{h=-\frac{N}{2},\ldots,\frac{N}{2}-1;n=0,\ldots,K}$ where F_1 is the fundamental frequency, and N is the number of harmonics within the sampling frequency band. This corresponds to the span of the set of poles with multiplicity $K+1$ at N harmonic frequencies [9]. In this regard, O-splines are imaginary exponential splines, or Fourier splines and they hold the properties and theorems of exponential B-splines in [8].

The synthesis equation of the DTTFT performs a Taylor interpolation over the support of the spline, but with the estimated derivatives it is also possible to do Hermite interpolation between consecutive cyclic states. The state sampler endowed with the Hermite interpolator provides an optimal data compression algorithm for oscillations and reduces the computational cost with a sufficiently small error controlled by the order of the spline and the degree of the Hermite spline.

In what follows, DTTFT signal model is presented in Section II. Lowpass O-splines are obtained in closed-form in Section III, together with their derivatives and frequency responses. Then, harmonic O-splines are established in Section III-D. In Section IV, O-splines are used to analyze and reconstruct a sinusoid, to denoise a frequency modulated mode in a real power oscillation (PO) [17], [18], and to separate the oscillatory modes of a real blood pressure oscillometric waveform (BPOW) [19]. Finally, conclusions are presented at the end of the paper.

II. Discrete-Time Taylor-Fourier Transform

DTTFT O-splines were introduced in [10] in matrix form. In this paper, they are obtained in closed form. This formulation helps to reduce their computational complexity and provides a sequence of functions whose spectra converge to the ideal lowpass filter.

Taylor-Fourier signal model is obtained by relaxing the Fourier coefficients to complex time functions of the form $\xi_h(t) = a_h(t)e^{j\varphi_h(t)}$, which carry the *complex envelope* at each hth harmonic frequency. Hence, the extended Fourier signal model becomes:

$$x(t) = \sum_{h=-\infty}^{\infty} \xi_h(t) e^{j2\pi h F_1 t}, \quad -\frac{CT_1}{2} \le t \le \frac{CT_1}{2} \tag{1}$$

where F_1 is the fundamental frequency in Hz, T_1 is its period ($T_1 = \frac{1}{F_1}$) in seconds, and C is the number of cycles.

In this way, the harmonics become narrowband signals [20]. The complex envelope $\xi_h(t)$ at each harmonic frequency is then approached by the best Taylor polynomial of K-th degree

$$\xi_h^{(K)}(t) = \xi_h(t_0) + \dot{\xi}_h(t_0)(t-t_0) + \cdots + \xi_h^{(K)}(t_0)\frac{(t-t_0)^K}{K!}, \tag{2}$$

in the least mean squares (LMS) sense on each observation interval, centered at the time instance t_0.

By taking N samples per fundamental period, the synthesis equation of the DTTFT subspace can be written from (1) and (2) as follows:

$$\begin{aligned} x &= \Phi\xi \\ &= \begin{pmatrix} I \begin{pmatrix} W_N \\ W_N \\ \vdots \\ W_N \end{pmatrix} & T \begin{pmatrix} W_N \\ W_N \\ \vdots \\ W_N \end{pmatrix} & \cdots \frac{1}{K!}T^K \begin{pmatrix} W_N \\ W_N \\ \vdots \\ W_N \end{pmatrix} \end{pmatrix} \begin{pmatrix} \xi_N \\ \dot{\xi}_N \\ \vdots \\ \xi_N^{(K)} \end{pmatrix} \end{aligned} \tag{3}$$

where the $(K+1)N \times (K+1)N$ matrix Φ contains the basis vectors, and the parametric $N \times 1$ sub-vectors $\xi_N^{(k)}$, $k = 0, 1, \ldots K$, contain the first K derivatives of the harmonic dynamic phasors $\xi_N(h)$, $h = 0, \ldots, N-1$ in subvector ξ_N. The $N \times N$ submatrix W_N is the Fourier matrix of the Discrete Fourier Transform (DFT) with harmonic columns $w_h = e^{j\frac{2\pi}{N}hn}$; $h, n = 0, \ldots, N-1$. And finally $(K+1)N \times (K+1)N$ diagonal matrix T contains the samples of the first Taylor term in in an interval of $C = K+1$ fundamental cycles. See [10] for more details of this formulation.

Notice in (3) that by increasing the Taylor order K by one, the size of the model increases by N since each Taylor term affects the full set of harmonics, and therefore another fundamental cycle of data is needed at the bottom of the Φ matrix. The diagonal Taylor matrices perform the Hadamard products of the Taylor terms with the Fourier columns in W_N.

In [10], it was shown that matrix Φ can be factorized as follows:

$$\begin{aligned} \Phi &= \Upsilon\Omega \\ &= \begin{pmatrix} I & Y_1 & \ldots & \frac{1}{K!}Y_1^K \\ I & Y_2 & \ldots & \frac{1}{K!}Y_2^K \\ \vdots & \vdots & \ddots & \vdots \\ I & Y_C & \ldots & \frac{1}{K!}Y_C^K \end{pmatrix} \begin{pmatrix} W_N & 0 & \ldots & 0 \\ 0 & W_N & \ldots & 0 \\ \vdots & \vdots & \ddots & \vdots \\ 0 & 0 & \ldots & W_N \end{pmatrix}, \end{aligned} \tag{4}$$

This factorization is achieved because columns of W_N are periodic. Diagonal $N \times N$ submatrices Y_c, $c = 1, 2, \ldots, C$,

are consecutive submatrices through the diagonal of matrix T in (3). They contain successive pieces of one cycle (N samples) of the first Taylor term in T. The Hadamard product in (3) is obtained in (4) block by block, of each column of submatrices in Υ, with the diagonal submatrices W_N in $\mathbf{\Omega}$, reconstructing the corresponding vertical submatrices in (3).

The best LMS coefficients of the projection of x onto the Taylor-Fourier subspace are provided by the following equation:

$$\widehat{\xi} = \widetilde{\Phi}^H x \tag{5}$$

in which $\widetilde{\Phi}$ is the dual matrix [21] of Φ, which is given by

$$\widetilde{\Phi} = \Phi(\Phi^H \Phi)^{-1}. \tag{6}$$

For $\Phi = \Upsilon\mathbf{\Omega}$ in (4), we have:

$$\widetilde{\Phi} = \Upsilon(\Upsilon^H \Upsilon)^{-1} \frac{\mathbf{\Omega}}{N} = \widetilde{\Upsilon} \frac{\mathbf{\Omega}}{N}, \tag{7}$$

which means that columns in $\widetilde{\Phi}$ are harmonic modulations of columns of diagonal submatrices in $\widetilde{\Upsilon}$, i. e. each column of diagonal submatrices in $\widetilde{\Upsilon}$ contain a common envelope (the lowpass O-spline and derivatives) modulated at the set of harmonic frequencies in W_N.

Since Υ is an invertible square matrix, its dual is simply the transpose of its inverse:

$$\widetilde{\Upsilon} = \Upsilon^{-T} = \frac{Adj(\Upsilon)^T}{|\Upsilon|}, \tag{8}$$

which is simply the matrix of cofactors $Adj(\Upsilon)^T$ divided by the determinant $|\Upsilon|$.

The multiplication of diagonal submatrices Y_i^k in the Taylor operator Υ yields the pointwise product of their diagonals. In consequence, Υ can be compacted in a $C \times C$ matrix by substituting each diagonal submatrix Y_i^k by the kth Taylor term as a time function evaluated on its corresponding ith segment. The inverse of that compact matrix can then be easily obtained since those functions perform as cofactors in the inversion.

In the following section, the Kth lowpass O-spline and its first derivatives are obtained in closed-form from the numerator in (7) when each submatrix W_N in $\mathbf{\Omega}$ is reduced to its first column of ones. The obtained submatrix is denoted by $\widetilde{\Phi}_0$ since this operation converts the diagonals in each row of $\widetilde{\Upsilon}$ into a vector that concatenates such diagonals in a piecewise polynomial. Diagonals in the first row provide the spline, and those of subsequent rows its first derivatives. Bandpass or harmonic O-splines are simple modulations of the lowpass O-spline and its derivatives at each harmonic frequency.

III. Lowpass O-Splines in Closed Form

In the following subsections we obtain the lowpass O-splines and first derivatives in $\widetilde{\Phi}_0$ by solving in colsed-form the inverse matrix of Υ in (8) and by concatenating each one of its rows in one vector of $\widetilde{\Phi}_0$. These vectors contain the common envelopes shared by the harmonic O-splines.

For $K = 0$, we have: $t_1 = t_{[-\frac{T_1}{2}, \frac{T_1}{2})}$ and $\Phi_0^{(0)} = 1$, and therefore $\widetilde{\Phi}_0^{(0)} = 1$. The system is orthogonal and the O-spline is a rectangular pulse.

$$\widetilde{\varphi}_0^{(0)}(t) = \begin{cases} 1 & -\dfrac{T_1}{2} \le t \le \dfrac{T_1}{2}, \\ 0 & \text{otherwise.} \end{cases} \tag{9}$$

For $K = 1$, $t_1 = t_{[-T_1,0)}$, and $t_2 = t_{[0,T_1)} = t_1 + T_1$, we have

$$\Phi_0^{(1)} = \begin{pmatrix} 1 & t_1 \\ 1 & t_2 \end{pmatrix} \tag{10}$$

with $|\Phi_0^{(1)}| = t_2 - t_1 = T_1$. Then, we have:

$$\widetilde{\Phi}_0^{(1)} = \frac{\begin{pmatrix} t_2 & -1 \\ -t_1 & 1 \end{pmatrix}}{T_1} = \begin{pmatrix} u_1 + 1 & -F_1 \\ -(u_2 - 1) & +F_1 \end{pmatrix} \tag{11}$$

where u_n is the normalized time: $u = t_n / T_1$. Its columns are a triangular pulse:

$$\widetilde{\varphi}_0^{(1)}(u) = \begin{cases} u + 1 & \text{for} \quad -1 \le u < 0, \\ 1 - u & \text{for} \quad 0 \le u < 1, \\ 0 & \text{otherwise,} \end{cases} \tag{12}$$

and the scaled Haar wavelet: $-F_1 \dot{\widetilde{\varphi}}_0^{(1)}(u)$.

For $K = 2$, we have

$$\Phi_0^{(2)} = \begin{pmatrix} 1 & t_1 & t_1^2/2 \\ 1 & t_2 & t_2^2/2 \\ 1 & t_3 & t_3^2/2 \end{pmatrix}. \tag{13}$$

with $t_1 = t_{[-\frac{3T_1}{2}, -\frac{T_1}{2})}$, $t_2 = t_1 + T_1$, and $t_3 = t_1 + 2T_1$. In this case $|\Phi_0^{(2)}| = T_1^3$, and

$$\widetilde{\Phi}_0^{(2)} = \begin{pmatrix} \dfrac{1}{2}(u_1 + 2)(u_1 + 1) & -F_1(u_1 + \dfrac{3}{2}) & F_1^2 \\ -(u_2 + 1)(u_2 - 1) & 2F_1 u_2 & -2F_1^2 \\ \dfrac{1}{2}(u_3 - 1)(u_3 - 2) & -F_1(u_3 - \dfrac{3}{2}) & F_1^2 \end{pmatrix}. \tag{14}$$

Notice in (11) and (14), that is sufficient to calculate the first column of the dual matrix, since the following ones are the negative derivative of the previous one scaled by constant factors. In fact, since the first column has even symmetry, only its first half is needed.

From (13) it can be seen that $\Phi_0^{(K)}$ is a Vandermonde matrix with scaled columns. In Appendix A it is proved that its determinant is $|\Phi_0^{(K)}| = T_1^{\frac{K(K+1)}{2}}$.

Finally, for $K = 3$, $t_1 = t_{[-2T_1,-T_1)}$ and $t_n = t_1 + (n-1)T_1$ $n = 2, 3, 4$. We have $|\Phi_0^{(3)}| = T_1^6$. Its first dual column is:

$$\widetilde{\varphi}_0^{(3)}(u) = \begin{cases} \dfrac{1}{6}(u + 3)(u + 2)(u + 1) & \text{for} -2 \le u < -1, \\ -\dfrac{1}{2}(u + 2)(u + 1)(u - 1) & \text{for} -1 \le u < 0, \\ \dfrac{1}{2}(u + 1)(u - 1)(u - 2) & \text{for} \quad 0 \le u < 1, \\ -\dfrac{1}{6}(u - 1)(u - 2)(u - 3) & \text{for} \quad 1 \le u < 2, \\ 0 & \text{otherwise.} \end{cases} \tag{15}$$

and the following ones are: $-F_1 \dot{\widetilde{\varphi}}_0^{(3)}$, $F_1^2 \ddot{\widetilde{\varphi}}_0^{(3)}$, and $-F_1^3 \dddot{\widetilde{\varphi}}_0^{(3)}$.

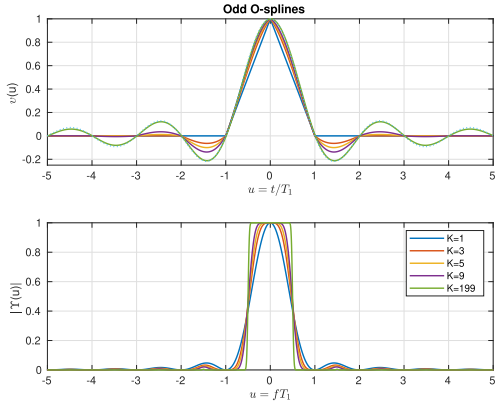

Fig. 1. Odd order lowpass O-splines and their spectra at the bottom.

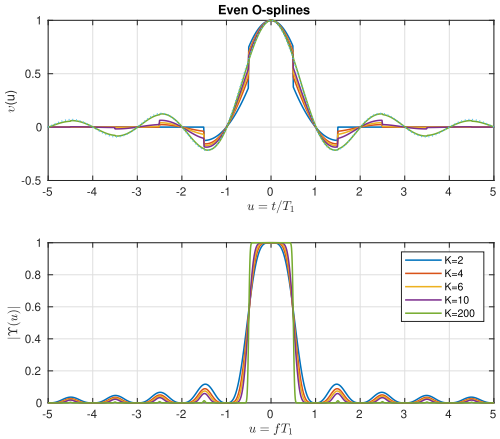

Fig. 2. Even order lowpass O-splines and their spectra at the bottom.

1) Kth Lowpass O-Splines in Factored Form: In general, the polynomial in the cth time interval from left to right of the Kth lowpass O-spline is given by

$$p_c(u) = \frac{1}{D_c} \prod_{\substack{n=1 \\ n \neq c}}^{K+1} (u + n - c), \quad c = 1, 2, \ldots, K+1 \tag{16}$$

in which the constant D_c guarantees unit value at $u = 0$ for each polynomial. One can recognize that the set of polynomials in (16) coincides with the set of Kth Lagrange polynomials interpolating a Dirac Kronecker sequence in windows of size K containing its central unit value. The lowpass O-spline is tiled with a piece of each of those polynomials, and it is identical to the Kth Lagrange central interpolation kernel [12]. The factored form in (16) allows the calculation of any O-spline, piece by piece, avoiding the singularity problem found in the inversion of the numeric Taylor operator in (8) when T_1 is small.

In [12], [22] and [23] is shown that any piece of the Lagrange central interpolation kernel converges to the corresponding piece of the *Sinc* function.

A. Lowpass O-Splines and Frequency Responses

The top plot in Fig. 1 illustrates several odd-order lowpass O-splines, together with the *Sinc* function, and their corresponding spectra are represented at the bottom. As can be seen, they provide a family of finite impulse response FIR filters that converge to the ideal lowpass filter. Each polynomial piece approximates a lobe of the *Sinc* function. The frequency response has a monotonic bandpass gain and small ripples on the stopband, similar to the IIR Type II Chebyshev filters. Even order lowpass O-splines also converge to the *Sinc* function but with discontinuities that produce higher ripples in their stopband as can be seen in Fig. 2.

Fig. 3 shows the spectra of odd O-splines in the bottom plot of Fig. 1, but in dB to assess their performance in harmonic analysis. For $K = 200$, the approximation to the ideal lowpass filter is quite remarkable, since the first sidelobe gain is at -47dB, and the stopband gains are at -326dB, and for $K = 9$ they are at -34 dB and -350dB, respectively.

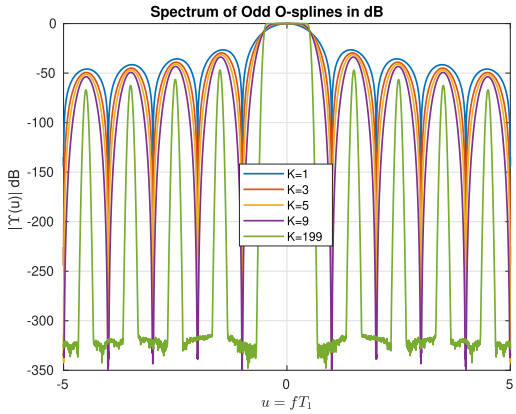

Fig. 3. Odd order lowpass O-splines and their spectra in dB.

Finally, comparing quadratic and cubic MK-splines with the same support cubic and quintic O-splines in Fig. 4, it is found that both types have flat passband, with the wider flat gain for the quintic O-spline. The first sidelobe of the MKs is at -32 and -42 dB, while that of the Os is at -30 and -31.5 dB, respectively. However, MK-splines have not maximally flat stopbands at harmonics as the O-splines do. Measured at the first harmonic the gains are at -60 and -64 dB for the MKs and at -223 and -322 dB for the Os, respectively. This property is crucial in harmonic analysis.

B. Lowpass O-Spline and Their Derivatives

For a given order, the dual matrix carries not only the lowpass O-spline but also its derivatives. The first row of plots in Fig. 5 shows the first lowpass O-splines and their columns the derivatives with increasing order from top to bottom.

By using a vertical set as impulse responses in a filter bank, they perform state sampling (or resampling). Notice that successive derivatives of an O-spline are linear combinations of translates of the precedent ones, forming a ladder of subspaces since successive derivatives are in state subspaces of the lower level. The last derivative in the diagonal constitutes the subspace with the inferior level V_0, spanned by translates of $\varphi_0^{(0)}(t)$, then the elements in the first supra-diagonal are

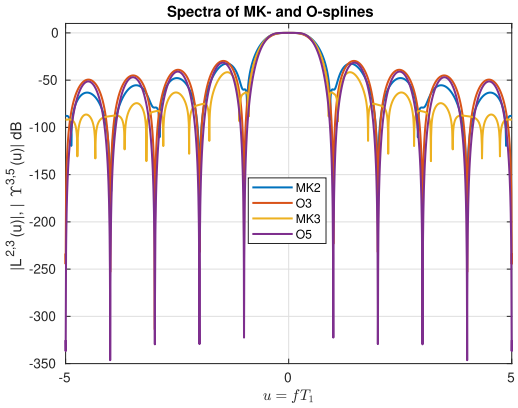

Fig. 4. Quadratic and cubic MK-splines compared with cubic and quintic O-splines.

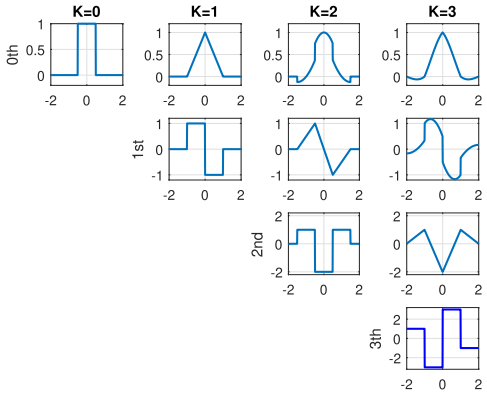

Fig. 5. At the top, the K-th lowpass O-splines for $K = 0, 1, 2$, and, 3, and their derivatives at the bottom.

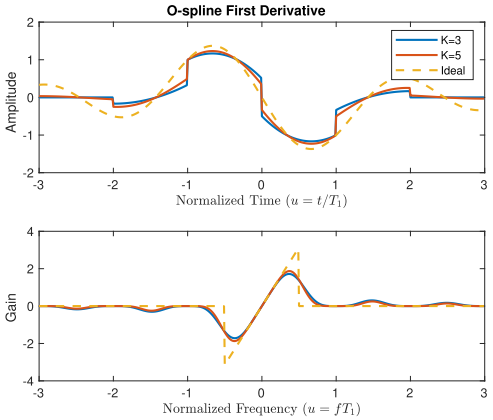

Fig. 6. Impulse and frequency responses of the first differentiators for $K = 3$, $K = 5$, and the ideal one in dashed line.

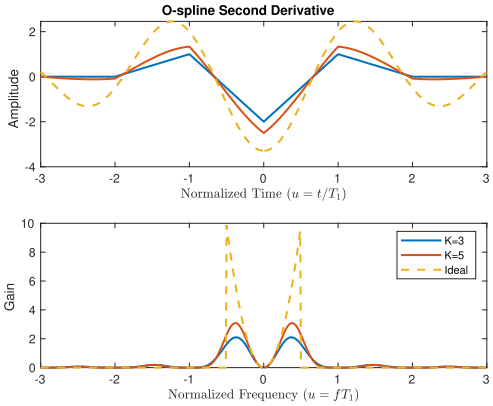

Fig. 7. Impulse and magnitude responses of the second differentiators, for $K = 3$, and the ideal one in dashed line.

in V_1, the subspace of linear piecewise functions, spanned by translates of $\varphi_0^{(1)}$, and so on, up to the O-spline with the highest grade.

For the third O-spline, we have the following derivatives in terms of lower degree O-splines:

$$\dot{\varphi_0}^{(3)}(u) = F_1[\varphi_0^{(2)}(u+\frac{1}{2}) - \varphi_0^{(2)}(u-\frac{1}{2})], \tag{17}$$

its second derivative:

$$\ddot{\varphi}_0^{(3)}(u) = F_1^2[\varphi_0^{(1)}(u+1) - 2\varphi_0^{(1)}(u) + \varphi_0^{(1)}(u-1)] \tag{18}$$

and its third derivative:

$$\dddot{\varphi}_0^{(3)}(u) = F_1^3[\varphi_0^{(0)}(u+\frac{3}{2}) - 3\varphi_0^{(0)}(u+\frac{1}{2}) + 3\varphi_0^{(0)}(u-\frac{1}{2}) - \varphi_0^{(0)}(u-\frac{3}{2})]. \tag{19}$$

C. Impulse and Frequency Response of Differentiators

The top curve of Fig. 6 shows the impulse responses of 3rd and 5th first differentiators, $\dot{\tilde{\varphi}}_0^{(3)}(u)$, and $\dot{\tilde{\varphi}}_0^{(5)}$. They converge to the derivative of the *Sinc* function shown with dashed line; while their frequency responses, at the bottom, converge to that of an ideal bandpass first differentiator. Indeed, if $H_h^{(0)}(f)$ is the frequency response of the h-th O-spline, then the first differentiator frequency response is $H_h^{(1)}(f) = (j2\pi f)H_h^{(0)}(f)$, i.e. a linear gain truncated by the frequency response of the hth O-spline, as shown by the dashed line.

Similarly, the impulse responses of the second differentiators $\ddot{\tilde{\varphi}}_0^{(3)}(u)$, and $\ddot{\tilde{\varphi}}_0^{(5)}$ are shown in the top curve of Fig. 7. As $K \to \infty$ they converge to the second derivative of the *Sinc* function; while their frequency responses, at the bottom, have a truncated parabolic gain on their passband. The frequency response of the second differentiator is $H_h^2(f) = (j2\pi f)^2 H_h^0(f)$, i.e. a truncated quadratic gain, as shown by the dashed line.

D. Harmonic O-Splines

Harmonic O-splines are simply modulated versions of the lowpass splines at a particular harmonic frequency. We have:

$$\tilde{\varphi}_h^{(K)}(u) = \tilde{\varphi}_0^{(K)}(u)e^{j2\pi hu}, \quad h = 0, 1, \ldots, N-1. \tag{20}$$

The zero-crossings of the complex exponential function coincide with those of the O-splines, preserving its cyclic property.

IV. Results

In this section, 3rd O-splines are used as samplers of a sinusoid of low frequency and its derivatives, in the extraction of a frequency modulated mode of a real power system [10],

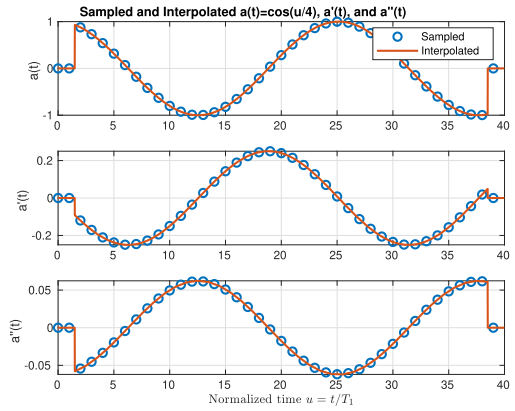

Fig. 8. Sampled and interpolated cosine function (top) and its first two derivatives (middle and bottom).

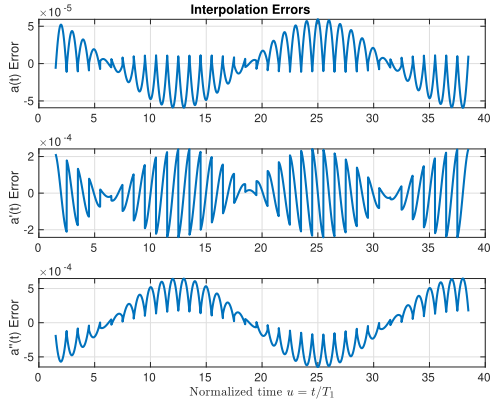

Fig. 9. Error of the synthetized signal, first and second derivatives with the Taylor signal model.

and in the analysis of oscillatory modes in the blood pressure oscillographic waveform (BPOW) [24]. Real signals with strong frequency fluctuations are used to assess the performance of the proposed method in real scenarios. The O-spline samplers are applied every fundamental cycle, and Taylor or Hermite interpolation is applied in the reconstructed signals.

A. Sampled and Interpolated Signals

The continuous sinusoidal signal $s(u) = cos(u/4)$ and its first two derivatives are analyzed and reconstructed with the proposed method. Since its spectrum is located under the ideal differentiator gains, the interpolation errors are small. This illustrates the good performance of the proposed technique. The top plot of Fig. 8 shows the signal and its first two derivatives with the corresponding estimated samples marked with circles. The standard deviation of the sampling errors is of 4.2×10^{-5}, 1.05×10^{-5}, and 4.59×10^{-4} for the function, first and second derivative, respectively. The interpolation errors achieved when those samples are interpolated with Taylor interpolations of 3rd, 2nd and 1st order are shown in Fig. 9. The obtained maxima interpolation errors are 6×10^{-5}, 2.1×10^{-4}, and 5×10^{-4}, respectively.

In addition to the Taylor interpolation, the signal samples are interpolated with the quintic Hermite scheme (Appendix B),

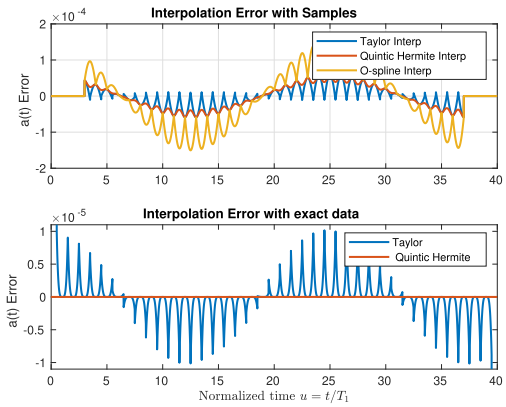

Fig. 10. Interpolation errors with samples and with exact data.

with the O-spline, and with the Keys cubic spline [25]. The interpolation errors are shown in the top plot of Fig. 10 and compared with the Taylor interpolation error. The smaller maximum error is achieved with the Taylor interpolation (with a maximum error of $\pm 6 \times 10^{-5}$) and with the quintic Hermite interpolation which is almost the envelope of the Taylor error and then followed by the O-spline with a maximum error of about 1.4×10^{-4}. The worst interpolation error is achieved by the Keys cubic spline, with a maximum error of 1.2×10^{-2}, which is even out of the range of the former ones.

To evaluate the performance of the optimal proposed method, the error achieved with the Taylor and the quintic Hermite interpolators when the exact samples of the function and derivatives are used is plotted at the bottom plot of Fig. 10. Both Taylor and Hermite error are zero flat around the poles. The maximum Taylor error is of 10^{-5}, while the Hermite one 5×10^{-9}. By comparing this plot with the top one in Fig. 9, it can be seen that the proposed method achieves an error only six times greater than the theoretical one with the same order $K = 3$.

B. Power Oscillation

The power oscillation analyzed in [10] is taken as a second example. It is obtained from three-phase voltages and currents, sampled at 20 samples per fundamental period, in a power system of $50Hz$, and illustrated in the top plot of Fig. 11, with its spectrum in the middle. The 3rd O-spline with time compression of two, and a bandwidth of 100Hz as shown at the bottom, is used to extract the oscillation. In [10] it is demonstrated that it is in fact a frequency modulated mode, going from zero to 15.6Hz.

The signal is sampled each half fundamental cycle using (5) and then Taylor interpolated in those intervals with (3). The result is shown in Fig. 12. The top plot shows the interpolated mode with Taylor polynomials. Its varying frequency is apparent since the period of the oscillation diminishes very fast at the end of the window, therefore the noise at the middle plot is just the difference between the original signal and the interpolated one. The bottom plot shows the reconstructed signal superposed to the original one. The reconstruction is almost perfect despite the high noise localized mainly during

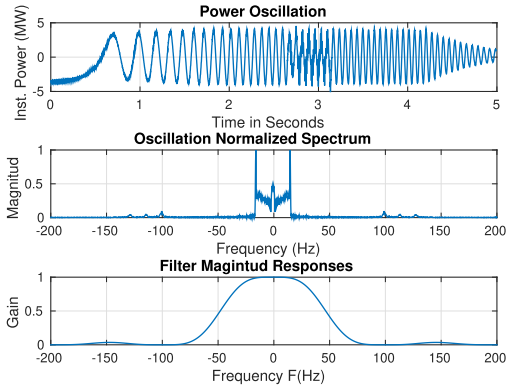

Fig. 11. PO (top plot) and its spectrum (middle plot), and frequency response of interpolating filter (at the bottom).

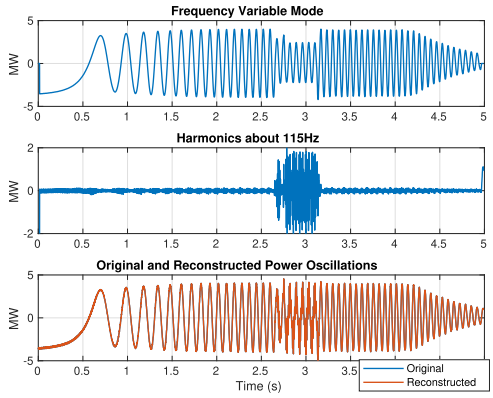

Fig. 12. Frequency modulating mode (top plot) and harmonics about $115Hz$ (middle plot), with the original and reconstructed PO.

the fault. The variance of the difference between the Taylor interpolated power oscillation and its instantaneous estimates obtained with the O-spline state sampler applied in successive time instances is equal to 0.0127, which is lower than the 0.32% of the maximum amplitude of the oscillation.

C. Blood Pressure Oscillometric Waveform

Estimation of systolic and diastolic blood pressure from numerical records of BPOWs [24] is an interesting challenge due to the complex structure of these signals. The extraction of the fundamental mode is crucial since it shows the main pulsation of the heart. Both pressures are estimated from its amplitude envelope. The other modes arise due to the non-linearity of the cuff.

The top plot of Fig. 13 shows the analyzed BPOW signal, sampled at 150 samples per second. Its basic temporal structure consists of repetitive peaks with hanging parabolic shapes, jumping up and down. Its spectrum is shown at the bottom with the frequency responses of the harmonic splines used in the decomposition. They are obtained by modulating (as indicated in III-D) the lowpass 3th O-spline dilated twice (8-cycles width) to halve its bandwidth. Samples are obtained by the dot product of the signal with successive translates of the corresponding harmonic 3rd O-splines and derivatives, and modes are reconstructed by its instantaneous ξ estimates.

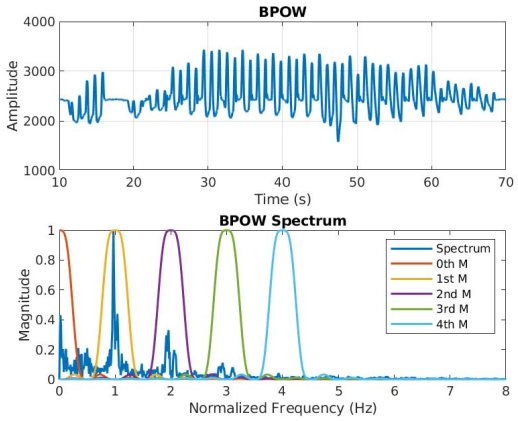

Fig. 13. BPOW (top), its spectrum and filter bank frequency responses (bottom).

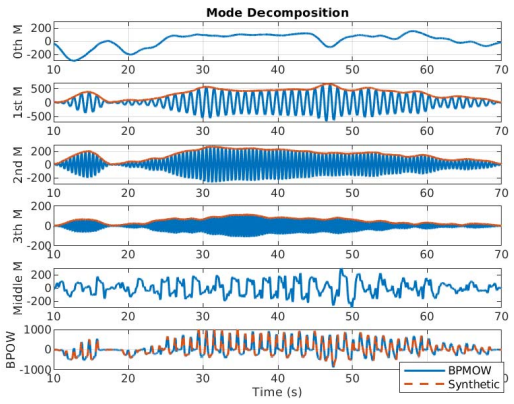

Fig. 14. Oscillographic decomposition of the BPOW. From top to bottom the predominant modes (0th,1st,2nd, and 3rd) followed by the signal with inter-harmonic frequencies. At the bottom, the synthetic signal with perfect reconstruction.

TABLE I

NORMALIZED MEAN SQUARED ERROR AS CONSECUTIVE MODES ARE TAKEN INTO ACCOUNT

Mean Squared Error (%)					
0th	1st	2nd	3rd	4th	Residual
87.64	31.22	19.08	17.19	17.00	0.00

BPOW predominant modes are shown in the first plots of Fig. 14, followed by the residual signal, and finally, at the bottom, the synthetic signal is compared with the original one. Notice that the 0th mode oscillates at a very low frequency. The envelope of the first mode has the expected parabolic shape. On the other hand, the residual signal has the crankshaft shape that explains the jumps of the parabolic shapes in the top plot of Fig. 13.

Table I shows the mean squared error (MSE) as a percentage of the BPOW energy as consecutive modes are aggregated into the reconstructed signal, achieving perfect reconstruction when all the components are included. Discrepancies are due to the complexity of the fluctuations of the BPOW signal, whose modes are not perfectly band-limited, as can be seen in the bottom plot of Fig. 13.

V. Discussion

The Lagrange central interpolation kernel is used in the literature as an interpolator [14], [22] or as a kernel approximating the Sinc function [12], but not as an analysis kernel, and much less as state-space sampler. This is the contribution of this paper, together with the closed-form derivation of the O-spline functions, which reduces the computational complexity of the DTTFT, especially when the signal has few harmonics, as the cases illustrated in the former section.

In [12] the interpolatory performance of the Lagrange central interpolation kernel and the fundamental cardinal spline [6] of successive orders is compared. However, this comparison is invalid in the analysis application since fundamental splines have infinite support, while the Lagrange kernels have a finite one.

The proposed method differs also from the one in [13], since the dual function of the interpolatory basis has not finite support. It also differs from the one used in [10], in which only the analysis equation (5) is used with O-spline and derivatives.

VI. Conclusion

O-splines are the impulse response of the DTTFT bandpass filters. They are modulations of the lowpass O-spline at the harmonic frequencies. They perform as ideal lowpass and bandpass filters with ideal differentiator gains and are used as optimal space samplers of band-limited signals, providing an optimal data compression algorithm for oscillations, with a sufficiently small error graduated by the degree of the spline. They are very useful to catch oscillations and in applications in which not only the signal but also its derivatives need to be estimated or interpolated, offering a powerful optimal state estimator implemented by FIR filters.

Appendix A
Vandermode Matrix Determinant

Given the Vandermode Matrix:

$$V_K = \begin{pmatrix} 1 & c_1 & c_1^2 & \dots & c_1^{K-1} \\ 1 & c_2 & c_2^2 & \dots & c_2^{K-1} \\ \vdots & \vdots & \vdots & \ddots & \vdots \\ 1 & c_K & c_K^2 & \dots & c_K^{K-1} \end{pmatrix}, \tag{21}$$

it is known that:

$$\det(V_K) = [\prod_{k=1}^{K-1} (c_K - c_{K-k})] \det(V_{K-1}). \tag{22}$$

In the case of $\Phi_0^{(K)}$, $t_K - t_{K-k} = kT$, and

$$\det(\Phi_0^{(K)}) = T^K \det(\Phi_0^{(K-1)}) \tag{23}$$

since the factorials of Taylor terms in columns of $\Phi_0^{(K)}$ cancel the factorials in the determinant of the Vandermonde matrix. Therefore:

$$\det(\Phi_0^{(K)}) = T^K T^{K-1} T^{K-2} \cdots T^2 T = T^{\frac{K(K+1)}{2}}. \tag{24}$$

with $\det(\Phi_0^{(0)}) = 1$.

Appendix B
Quintic Hermite Interpolator

We have:

$$f(x) = y_0\varphi_0(u) + \dot{y}_0\varphi_1(u) + \ddot{y}_0\varphi_2(u) \tag{25}$$

$$+ y_1\varphi_3(u) + \dot{y}_1\varphi_4(u) + \ddot{y}_1\varphi_5(u) \tag{26}$$

with:

$$\varphi_0(u) = 1 - 10u^3 + 15u^4 - 6u^5 \tag{27}$$

$$\varphi_1(u) = u - 6u^3 + 8u^4 - 3u^5 \tag{28}$$

$$\varphi_2(u) = (u^2 - 3u^3 + 3u^4 - u5)/2 \tag{29}$$

$$\varphi_3(u) = 10u^3 - 15u^4 + 6u^5 \tag{30}$$

$$\varphi_4(u) = -4u^3 + 7u^4 - 3 * u^5 \tag{31}$$

$$\varphi_5(u) = (u^3 - 2u^4 + u^5)/2. \tag{32}$$

References

[1] C. de Boor, *A Practical Guide to Splines*. Springer, 2001.

[2] I. J. Schoenberg, *Cardinal Spline Interpolation*. Philadelphia, PA, USA: SIAM, 1973.

[3] D. Pang, L. A. Ferrari, and P. V. Sankar, "B-spline FIR filters," *Circuits Syst. Signal Process.*, vol. 13, no. 1, pp. 31–64, Mar. 1994, doi: 10.1007/BF01183840.

[4] T. M. Lehmann, C. Gonner, and K. Spitzer, "Survey: Interpolation methods in medical image processing," *IEEE Trans. Med. Imag.*, vol. 18, no. 11, pp. 1049–1075, Nov. 1999.

[5] S. G. Mallat, "A theory for multiresolution signal decomposition: The wavelet representation," *IEEE Trans. Pattern Anal. Mach. Intell.*, vol. 11, no. 7, pp. 674–693, Jul. 1989.

[6] M. Unser, A. Aldroubi, and M. Eden, "B-spline signal processing. I. Theory," *IEEE Trans. Signal Process.*, vol. 41, no. 2, pp. 821–833, Feb. 1993.

[7] M. Unser, A. Aldroubi, and M. Eden, "B-spline signal processing. II. Efficiency design and applications," *IEEE Trans. Signal Process.*, vol. 41, no. 2, pp. 834–848, Feb. 1993.

[8] M. Unser and T. Blu, "Cardinal exponential splines: Part I—Theory and filtering algorithms," *IEEE Trans. Signal Process.*, vol. 53, no. 4, pp. 1425–1438, Apr. 2005.

[9] M. Unser, "Cardinal exponential splines: Part II—Think analog, act digital," *IEEE Trans. Signal Process.*, vol. 53, no. 4, pp. 1439–1449, Apr. 2005.

[10] J. A. de la O Serna, "Analyzing power oscillating signals with the O-Splines of the discrete Taylor–Fourier transform," *IEEE Trans. Power Syst.*, vol. 33, no. 6, pp. 7087–7095, Nov. 2018.

[11] J. A. de la O Serna, M. R. A. Paternina, A. Zamora-Mendez, R. K. Tripathy, and R. B. Pachori, "EEG-rhythm specific Taylor–Fourier filter bank implemented with O-Splines for the detection of epilepsy using EEG signals," *IEEE Sensors J.*, vol. 20, no. 12, pp. 6542–6551, Jun. 2020.

[12] E. H. W. Meijering, W. J. Niessen, and M. A. Viergever, "The sinc-approximating kernels of classical polynomial interpolation," in *Proc. Int. Conf. Image Process.*, vol. 3, Oct. 1999, pp. 652–656.

[13] M. Unser and A. Aldroubi, "A general sampling theory for nonideal acquisition devices," *IEEE Trans. Signal Process.*, vol. 42, no. 11, pp. 2915–2925, Nov. 1994.

[14] E. Meijering, "A chronology of interpolation: From ancient astronomy to modern signal and image processing," *Proc. IEEE*, vol. 90, no. 3, pp. 319–342, Mar. 2002.

[15] J. Chen and Z. Cai, "Cardinal MK-spline signal processing: Spatial interpolation and frequency domain filtering," *Inf. Sci.*, vol. 495, pp. 116–135, Aug. 2019. [Online]. Available: http://www.sciencedirect.com/science/article/pii/S0020025519303767

[16] J. Chen and Z. Cai, "A new class of explicit interpolatory splines and related measurement estimation," *IEEE Trans. Signal Process.*, early access, Apr. 2020, doi: 10.1109/TSP.2020.2984477.

[17] G. Rogers, *Power System Oscillations*. Boston, MA, USA: Springer, 2000.

[18] A. R. Messina, *Inter-area Oscillations in Power Systems: A Nonlinear and Nonstationary Perspective*. New York, NY, USA: Springer, 2009.

[19] M. Forouzanfar, H. R. Dajani, V. Z. Groza, M. Bolic, S. Rajan, and I. Batkin, "Oscillometric blood pressure estimation: Past, present, and future," *IEEE Rev. Biomed. Eng.*, vol. 8, pp. 44–63, 2015.
[20] J. G. Proakis and M. Salehi, *Digital Communications*, 5th ed. Boston, MA, USA: McGraw-Hill, 2008, sec. 2.1.
[21] M. Vetterli, K. Kovacevic, and V. K. Goyal, *Foundations of Signal Processing*, 3rd ed. Cambridge, U.K.: Cambridge Univ. Press, 2014. [Online]. Available: http://www.fourierandwavelets.org/
[22] H. W. Meijering. *Image Enhancement in Digital X-Ray Angiography*. Accessed: May 28, 2020. [Online]. Available: https://dspace.library.uu.nl/bitstream/handle/1874/367/c6.pdf
[23] A. K. Jain, *Fundamentals of Digital Image Processing*. Englewood Cliffs, NJ, USA: Prentice-Hall, 1989.
[24] J. A. de la O Serna, "Taylor–Fourier analysis of blood pressure oscillometric waveforms," *IEEE Trans. Instrum. Meas.*, vol. 62, no. 9, pp. 2511–2518, Sep. 2013, doi: 10.1109/TIM.2013.2258245.
[25] R. Keys, "Cubic convolution interpolation for digital image processing," *IEEE Trans. Acoust., Speech, Signal Process.*, vol. 29, no. 6, pp. 1153–1160, Dec. 1981.

José Antonio de la O Serna (Senior Member, IEEE) received the Ph.D. degree from Telecom ParisTech, France, in 1982. In 1987, he joined the Ph.D. program in electrical engineering at the Autonomous University of Nuevo León (UANL), where he was a member of the Doctoral Committee. He was a Professor with the Monterrey Institute of Technology from 1982 to 1986. From 1988 to 1993, he was with the Electrical Department, Polytechnic School, Yaounde, Cameroon. He is currently a Research Professor with UANL, Monterrey, Mexico. He is a member of the Mexican Research System.